Tsunami Waves Generated by Cliff Collapse: Comparison Between Experiments and Triphasic Simulations

S. Viroulet, A. Sauret, O. Kimmoun and C. Kharif

Abstract Although many tsunamis arise from underwater earthquakes, some are induced by submarine and subaerial landslides. For example, the collapse of an unstable cliff into the sea can generate a tsunami wave near the coast and exhibit extreme run-up. As a result, those tsunamis develop significant hazards to the population. The threat caused by such tsunamis strongly depends on the topography and location of the unstable cliff. Predicting the height of the tsunami wave generated by a subaerial or submarine collapse requires experimental investigations, analytical modeling, and numerical simulations. In this chapter, we discuss recent experimental results on granular collapse in water and the influence of the physical parameters on the amplitude of the tsunami waves. We also present triphasic numerical simulations based on a finite-volume method where different rheologies are considered for the slide. We also emphasize the difficulty of such simulations and compare the numerical results to experimental measurements.

1 Introduction

A tsunami is an ocean wave that can propagate over long distances and can lead to considerable damage along the coast. Among all natural disasters, tsunamis can

S. Viroulet (✉)
School of Mathematics and Manchester Centre for Nonlinear Dynamics,
University of Manchester, Manchester, UK
e-mail: sylvain.viroulet@manchester.ac.uk

A. Sauret
Surface du Verre Et Interfaces, UMR 125 CNRS/Saint-Gobain, Aubervilliers, France
e-mail: alban.sauret@saint-gobain.com

O. Kimmoun · C. Kharif
Aix-Marseille Université, CNRS, Ecole Centrale Marseille, IRPHE UMR 7342, Marseille, France
e-mail: olivier.kimmoun@centrale-marseille.fr

C. Kharif
IRPHE, Ecole Centrale Marseille, 49 rue F. Joliot-Curie, 13384 Marseille cedex 13, France
e-mail: kharif@irphe.univ-mrs.fr

E. Pelinovsky and C. Kharif (eds.), *Extreme Ocean Waves*,
DOI 10.1007/978-3-319-21575-4_10

be one of the deadliest. Indeed, if the wave amplitude reaches 10 m in height when arriving near the coast, the subsequent flooding can devastate land over several kilometers.

The most common mechanism responsible for tsunami generation is a submarine earthquake (Ioualalen et al. 2007), but other geological events can also cause tsunamis. For instance, the impact of asteroids (Gisler et al. 2004; Kharif and Pelinovsky 2005), volcanic eruptions (Francis 1985; Choi et al. 2003), and landslides result in tsunamis that lead to important local hazards. Because the wavelengths associated with tsunamis generated by a landslide are significantly lower than those from tsunamis induced by a submarine earthquake, the dispersive effects are more important during the propagation of the former (Glimsdal et al. 2013). For this reason, it is common to call the waves generated by a landslide "impulse waves" rather than tsunamis. However, despite the larger dissipation, the amplitude of those impulse waves depends directly on the volume and configuration of the landslide, and can become much larger than tsunami wave generated by submarine earthquake (Fritz 2001).

Over the past twenty years, various studies have been performed to characterize the mechanisms involved in the generation of tsunamis by landslides. In some particular cases, the propagation of the generated waves can be described by the Saint-Venant equations (Popinet 2011) and in a more general framework, the Boussinesq equations are able to capture the propagation of an initial wave (Shi et al. 2011, 2012). Although the propagation is now well described, the initial generation of the waves remains poorly understood because of its complexity. Many experimental studies have characterized waves generated by a landslide. The simplest approach used a solid block to model the landslide (Scott 1845). The mathematical description was obtained fifty years later by Korteweg and De Vries (1895). To obtain a more realistic situation, a number of studies have later considered a solid triangular block, with a width equal to that of the channel, that slides on a slope and impacts into water (Heinrich 1992; Watts 1997, 1998, 2000). These studies quantified the amount of energy transferred from the solid block to the waves and derived scaling laws to estimate the amplitude of the generated waves. Walder et al. (2003) studied the tsunami generation by a solid block sliding in air on a varying slope allowing for a smooth transition between the slope and the bottom of the channel and avoid the impact between the solid block and the bottom of the channel.

Large-scale experiments were carried out by Liu et al. (2005) to study the run-up and rundown of waves generated by a 3D slide. This study showed that the run-up is significantly larger for subaerial slides and that it is controlled by the initial size and position of the slide. In parallel, Panizzo et al. (2005) have performed similar 3D experiments to predict the amplitude of the generated waves for the same parameters as Walder et al. (2003). Experiments at the 1:500 scale were performed by Sælevik et al. (2009) to estimate the amplitude of waves generated by the collapse of a cliff in the Akneset fjord in Norway. This study examined the influence of the length of the slide on the generated wave train. They used several solid blocks connected to each other, and observed that the total volume of the slide is the predominant parameter that controls the amplitude of the first wave, whereas the total length influences

the dispersive tail. They showed that the shorter the solid assembly, the larger the wave train following the first wave. Other configurations have also been studied to characterize the generation of tsunamis by a landslide. They consist in approximating the slide by a Gaussian or elliptical shape instead of a triangular or trapezoidal block (Grilli and Watts 2005; Enet et al. 2003, 2005, 2007). These experiments constitute validating cases for many numerical simulations of the generation of tsunamis by submarine landslides. Risio et al. (2009) considered the same geometry as Enet et al. (2007), but in order to study tsunami generation by a subaerial landslide. Contrary to previous studies, they focused on the water rise along the coast perpendicularly to the slide. They observed that the maximum run-up does not take place near the slide but at 2–3 times from its width.

Whereas the generation of tsunamis by a solid has been extensively studied since the 1970s, the generation of tsunamis by a granular slide is more recent and offers a more realistic approach. During the collapse of the slide, modeling of the interactions between the granular material and the generated wave is of crucial importance to estimate the initial amplitude of the tsunami. Various experiments using granular materials were carried out by Fritz (2002), Fritz (2001); Fritz et al. (2003a, b, 2004, 2009). These bi-dimensional experiments were performed in a 11m $\times$ 0.5m $\times$ 1m channel and the granular medium was initially accelerated using a pneumatic piston. Using linear regression, the authors determined the main characteristics of the generated waves based on several dimensionless parameters such as the Froude number $\mathrm{Fr} = \mathrm{V}/\sqrt{\mathrm{g}\,\mathrm{H}}$ (where V is the velocity of the slide, H is the water depth, and g is the gravitational acceleration). These experimental studies were followed by the experiments of Zweifel et al. (2006) that studied the effects of the density of the granular material. Heller et al. (2008) considered the scale effects of tsunamis generated by landslides. They found that the interfacial tension and viscous effects decrease the amplitude of the generated wave but only have a small influence on the speed of their propagation. More recently, Mohammed (2010) and Mohammed and Fritz (2012) performed large-scale experiments on tsunami generation by a 3D sliding granular material. The granular mass used in this study reaches a value of 1.4 tons and the Froude number at the impact varied between 1 and 4. They were able to obtain the evolution of the amplitude taking into account the direction of propagation of the wave compared to the direction of collapse.

Several analytical studies considered the influence of different parameters in tsunami generation by landslides. Murty (1979) calculated the amplitude of the wave generated by a submarine landslide assuming that the potential energy of the slide is entirely transferred to the solitary wave. This assumption of total transfer of energy was also used by Monaghan and Kos (2000) to predict the elevation of the free surface in the historical experiment of John Scott Russell. Later, Didenkulova et al. (2010) studied the generation and propagation of tsunami induced by a deformable landslide on a varying topography. They found that amplitude of the generated wave does not vary monotonically with the distance. Wang et al. (2011) suggested a formulation for the generation of tsunamis by strong submarine landslide, taking into account the effects of the wave, the viscous friction with the fluid and the solid friction with the bottom of the sliding solid. More recently, scaling laws predicting the evolution of a

wave have been obtained by Viroulet et al. (2013) for a solid slide and by Heller and Hager (2014) for a deformable slide.

Depth-averaged models have been widely used in numerical simulations of the tsunami propagation (Tinti and Bortolucci 2000). However, because these models neglect the vertical acceleration, they are not well suited to capture the generation of the initial wave by a landslide. Assier-Rzadkieaicz et al. (1997) used experimental results obtained with granular material to develop a simulation of the wave generation by a submarine landslide. Their code solved the Navier-Stokes equations by using a Bingham rheology to model the flow of granular material. Using the same rheology, Watts et al. (2003) simulated wave generated by submarine landslide and showed that the non-linearity and dispersion of the generated waves need to be taken into account in numerical models. These results have led to a numerical code, *Geowave*, which is the combination between two open-source codes: TOPICS, *Tsunami Open and Progressive Initial Condition Systems* Watts et al. (2003), that gives the initial conditions, and FUNWAVE, that solves the nonlinear Boussinesq equations for the propagation (Shi et al. 2011). Another numerical method particularly used to study tsunamis relies on the potential method, known as the *Boundary Elements Method* (BEM). Grilli and Watts (1999) developed a 2D code (2D-FNPF) to study the generation by a strong submarine landslide with a semi-elliptical shape. A 3D extension of this code was also performed by Grilli et al. (2002). However, depending on the initial depth of the submarine landslide, and in the case of a subaerial landslide, a strong vorticity is generated during the collapse and the possible fragmentation of the free surface can not be simulated using this method.

To take into account the interactions between the slide and the free surface, multiphase codes have recently been developed. Kelfoun et al. (2010) modeled the tsunami generation on the island of "La Réunion" by solving the Saint-Venant equations for both, the fluid and the slide with a Mohr-Coulomb friction law for the rheology of the slide. Other numerical codes have been developed by solving the Navier-Stokes equations for the three phases air/water/slide. Mader and Gitting (2002) used the SAGE code that relies on an adaptive mesh to solve the Navier-Stokes equations with a Godunov scheme. Quecedo et al. (2004) modeled the generation by a deformable landslide using a level-set method and a viscoplastic rheology.

More recently, Abadie et al. (2010) used a finite volume method to solve the Navier-Stokes equation and a Volume of Fluid method (VoF) to track the interfaces. Several types of rheology can be implemented in this code (THETIS). The authors applied this method to study the possible collapse of the Cumbre Vieja, a volcano located in the Canary Islands (Abadie et al. 2012). They coupled the multi-phasic tsunami generation, simulated with the code THETIS, with the propagation mechanism, simulated with the code FUNWAVE. This numerical study highlights the importance of the 3D effects during both the generation and the propagation phases. Their study showed that 2D numerical simulations largely overestimate the amplitude of the wave.

These different studies illustrate that a good modeling of the couplings between the slide and the wave is crucial to predict the hazards induced by landslide generated tsunamis with the most realistic model involving a granular medium to reproduce the

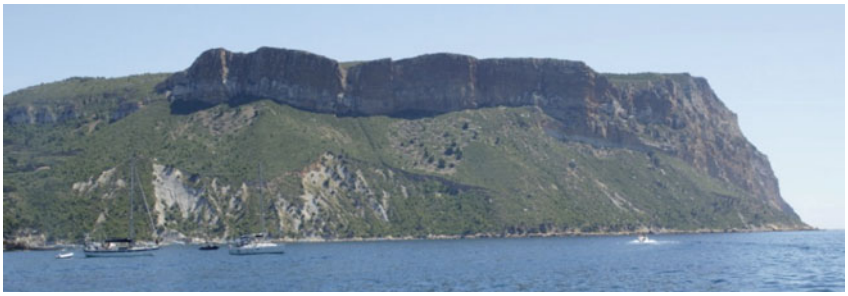

Fig. 1 A view of the cliff at Cap Canaille located just above the mediterranean sea in Cassis, France (picture: S. Viroulet)

deformable slide. However, the interactions of the landslide with the slope have not been considered, as most of the past studies considered situations at Froude number $\mathrm{Fr} > 1$, where the friction with the slope can be neglected. In particular, during the collapse of a cliff initially located just above the water surface, the velocity of the landslide is small compared to the speed of propagation of the generated wave and the interactions need to be characterized. This situation is observed for instance in Cassis (France) where the possible collapse of a cliff of more than 350 m high would occur directly above the water as illustrated in Fig. 1 (Averbukh et al. 2013).

2 Experimental Investigations

2.1 Experimental Setup

We have performed systematic experiments to study the interactions between dry granular collapse and water that generates impulse waves. An aquarium tank of dimension 220 cm in length, 40 cm in height and 20 cm in width was built so that it is long enough to allow the propagation of the wave while also allowing the observation of the interactions between granular collapse and the generated waves.

To characterize the influence of the granular medium on both the generated wave and the granular collapse, we have used four different media of varying size, polydispersity, and sphericity. We considered three sizes of spherical glass beads (1.5, 4, and 10 mm) and density $\rho_b = 2500\ \mathrm{kg.m^{-3}}$. We also used aquarium sand with an average diameter of 4 mm and density of $\rho_s = 2300\ \mathrm{kg.m^{-3}}$ that models a non-spherical and polydisperse medium. The reservoir of granular material was located on one side of the aquarium and was limited by a door that opens vertically. The velocity of the door was fast enough, around $2\ \mathrm{m.s^{-1}}$, to assume that the shape of the granular heap was not modified before the collapse. The granular material flows subsequently down the slope, where the same granular material has been glued to the surface to ensure a no-slip boundary condition (Pouliquen 1999; Cassar et al. 2005).

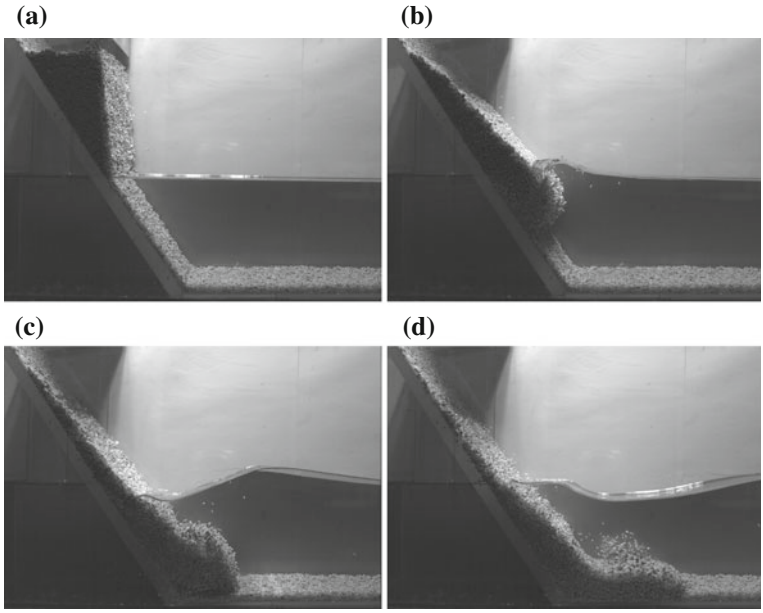

Fig. 2 Granular collapse of $m = 2$ kg of aquarium sand from air into water. The time step between two pictures is 0.2 s

The evolution of the granular collapse and the generation of the wave were recorded using a high speed camera (Vision Research Phantom V641) at a rate of 100 frames per second. In addition, we measured the evolution of the amplitude of the waves generated during the propagation using 4 resistive gauges placed at 0.45, 0.75, 1.05, and 1.35 m away from the vertical door (Viroulet et al. 2013a, b). An example of the results obtained with the high speed camera is shown in Fig. 2 for a collapse of aquarium sand.

2.2 Evolution of Amplitude During the Propagation of the Wave

We first focus on the propagation of the leading wave, which is followed by an oscillatory wave train. Because the wave generation is a complex phenomenon, prior to any systematic study, we ensured that the experiments were fully reproducible. Figure 3(a–d) report an example of the evolution of the wave amplitude at the four resistive gauges, for $m = 2$ kg of 4 mm glass beads on a slope of 45°. Whereas the free surface elevation remains relatively small ($\eta_{\max} < 2$ cm), the difference in elevation between the experiments is smaller than 1 mm. Therefore, the slight difference in compaction of the initial granular media or the variation of the velocity

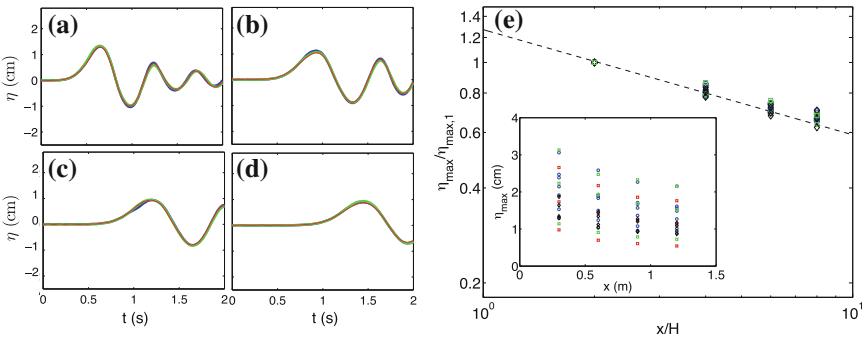

Fig. 3 Time evolution of the free surface elevation measured at the four resistive gauges placed at **a** 0.45 m, **b** 0.75 m, **c** 1.05 m, and **d** 1.35 m from the lifting gate. The granular collapse starts at time $t = 0$. The three curves (*red*, *green*, *blue*) correspond to replicate of the experiment performed with $m = 2$ kg of 4 mm glass beads sliding on a slope of 45°. **e** Evolution of the rescaled amplitude of the leading wave as a function of the rescaled distance of propagation for various masses (1, 2 or 3 kg), various slopes (35°, 40°, 45°, 50°, 55°), and four granular materials (glass beads of diameter 1.5, 4, and 10 mm and aquarium sands). Inset: Measured dimensional amplitude of the leading wave as a function of the distance of propagation

of the lifting gate do not significantly modify the experimental measurement. This result confirmed that our experimental setup can reliably be used to determine the amplitude of the wave generated by a granular collapse into water.

For each experiment, we rescale the amplitude of the wave at the probes by the amplitude η_{max_1} at the first probe (see Fig. 3e). To explain the dependence of the tsunami amplitude on the distance from the source x, we consider the weakly dispersive linear shallow water approximation. In this approximation, the free surface elevation η is described by the linearized Korteweg-de-Vries equation (Whitham 2011; Pelinovsky et al. 2000):

$$\frac{\partial \eta}{\partial t} + c\,\frac{\partial \eta}{\partial x} + \frac{c\,H^2}{6}\,\frac{\partial^3 \eta}{\partial x^3} = 0. \tag{1}$$

A solution to this equation is

$$\eta(x,t) = Q\left(\frac{2}{ct\,H^2}\right)^{1/3} \mathrm{Ai}\left[\left(\frac{2}{ct\,H^2}\right)^{1/3}(x - ct)\right], \tag{2}$$

where Q is a constant corresponding to the cross section of the volume of displaced water, H is the water depth, $c = \sqrt{gH}$ and Ai is the Airy function. Thus, during the propagation, the amplitude of the leading wave decays as $t^{-1/3}$, which leads to a dependence as $x^{-1/3}$. This scaling law is consistent with the experimental data regardless of the initial mass or slope (see Fig. 3e). Note also that the viscosity and the interfacial tension are expected to have negligible effects on the propagation of

the wave as observed for solid body impact (Viroulet et al. 2013) or granular impact at Fr $>$ 1 (Heller et al. 2008; Mohammed and Fritz 2012). Thus, using a far-field approximation, we can estimate the amplitude of the waves during propagation.

2.2.1 Amplitude of the Generated Waves

An important parameter to predict tsunamis generated by landslides is the volume of the slide. We performed a systematic investigation by varying the initial mass of the slide from 0.5 to 3 kg for the four granular media previously described. The other experimental parameters, i.e. the slope angle and the water depth are kept constant at 45° and 15 cm, respectively. We observe that the amplitude of the first wave increases with the mass of the slide (see Fig. 4a). Fitting the experimental measurements leads to a power law $\eta_{max_1} \propto m^{0.84}$ for the glass beads and $\eta_{max_1} \propto m^{0.95}$ for the aquarium sand. The experiments performed with the 4 mm and 10 mm glass beads lead to similar values. The exponent of the power law for the 1.5 mm glass beads is the same but the prefactor is slightly lower. Surface tension effects are likely a cause of this discrepancy. Indeed, the size of the beads should be compared with the capillary length in the system, $L_c = \sqrt{\sigma/\rho\, g} \simeq 2.7$ mm (where σ and ρ are the interfacial tension and the density of the water, respectively, g is the gravitational constant). Therefore, unlike in the propagation phase of the wave, the effects of the interfacial tension can be significant during the generation. We can reasonably assume that these effects are less important with the aquarium sand or large glass beads (10 mm) than for experiments with glass beads of 1.5 mm.

Predicting the influence of the mass of the slide on the amplitude of the first wave remains challenging. Indeed, an analysis based on the initial potential energy of the slide transferred to the first wave is not satisfying. When the mass of the slide is large (typically $>$ 2 kg in our setup), the leading wave starts to propagate while some

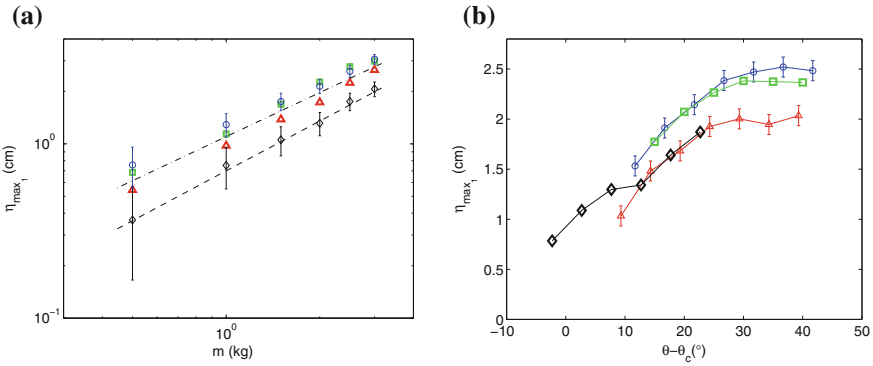

Fig. 4 **a** Evolution of the maximum amplitude at the first probe as a function of the mass of granular material. **b** Evolution of the amplitude of the leading wave as a function of $\theta - \theta_c$. (△: 1.5 mm glass beads, ○: 4 mm glass beads, □: 10 mm glass beads and ◊: aquarium sand)

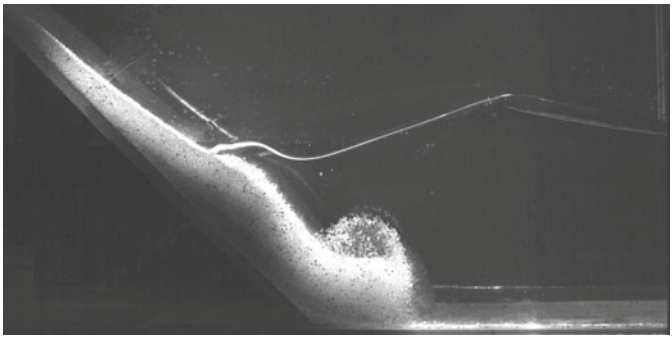

Fig. 5 Image of a granular collapse into water of 3 kg of 1.5 mm glass beads on a slope of 45° taken at $t = 0.45$ s

granular media is still out of the water. Therefore, all the mass of the material does not contribute to the generation of the first wave. This situation is illustrated in Fig. 5 where the first wave has left the region where the generation takes place while some granular material is still flowing down the slope.

The present observation can be related to the work of Sælevik et al. (2009) on the influence of the length of the slide which was solid in their case. Indeed, they observed that the length influences the dispersive wave train. In our situation, for a larger mass of granular material, the collapsing time is longer and an excess of granular material comes into play while generating the wave train following the first wave. The same explanation shows that the evolution of the amplitude of the first wave with the slide mass is almost independent of the material used. Indeed, the generation of the first wave is mainly caused by the impact into water and is roughly the same regardless of the granular media used.

An important parameter in geophysical situations is the angle of the slope. However, comparing the results for different granular materials is not straightforward as they flow at different angles. Therefore, we measured the angle of repose and avalanche of the four granular media (Börzsönyi et al. 2008). We find that the critical angles of avalanche θ_c differ by 17° between the glass beads and the aquarium sand. The evolution of maximum elevation of the free surface as a function of $\theta - \theta_c$ is illustrated in 4b (for more details see Viroulet et al. (2014)). We show that the amplitude of the first wave only depends on $\theta - \theta_c$. Again, the interfacial tension may explain the difference of the amplitude for the 1.5 mm glass beads. In this figure, we also observe a saturation of the amplitude of the first wave for $\theta - \theta_c \geq 30°$ for all granular media (note that for the aquarium sand these large values can not be achieved with our experimental setup).

We calculate the energy of the wave train associated to the first three waves (the energy contained in the following wave train can be reasonably neglected). The evolution of this energy E as a function of $\theta - \theta_c$ is shown in Fig. 6a. The experimental measurements collapse on a main curve and a transition is observed at $\theta - \theta_c \simeq 10°$. Note that these low values can not be achieved with our device for glass beads. Again,

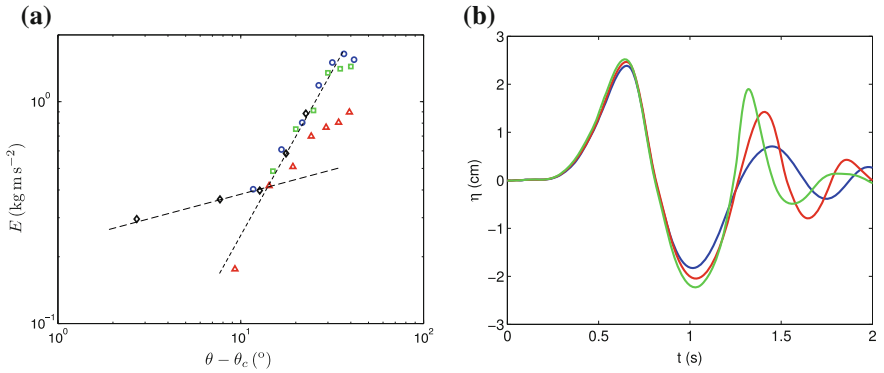

Fig. 6 **a** Evolution of the energy E in the wave train as a function of $\theta - \theta_c$ (△ : 1.5 mm glass beads, ○ : 4 mm glass beads, □ : 10 mm glass beads and ◊: aquarium sand). **b** Elevation of the free surface at the first probe for slopes of (-) 50°, (-) 55° and (-) 60°, a water depth equal to 0.15 m and 2 kg of 4 mm glass beads

the evolution of the energy of the wave train generated with 1.5 mm beads is slightly different from other granular materials, which confirms that the interfacial tension effects are important when the typical size of the granular material is smaller than the capillary length.

For all granular media, we observe that the total energy of the wave train increases with the slope and remains the same for $\theta - \theta_c > 30°$. This result seems contradictory with previous results on the amplitude of the first wave but can be explained using the measurement of the probes. Indeed, for large slope angles, the amplitude of the second wave becomes more important. In Fig. 6b, we report the evolution of the free surface at the first probe for three different slopes and 4 mm glass beads. Beyond a certain angle, the amplitude of the first wave does not increase anymore while the amplitude of the second wave increases. The energy and the amplitude of the first wave reach a saturation. However, the rest of the energy is found in the second wave which becomes as dangerous as the leading wave. Figure 6a shows that the last point obtained with the 4 mm glass beads becomes lower in energy for large slope angles. This is due to the large curvature of the second wave, which in this configuration breaks before reaching the probe, thereby decreasing the total energy of the wave train. When the slope increases and the energy of the first wave does not increase, the rest of the energy is transferred to the wave train and more particularly in the second wave.

3 Numerical Simulations

Our experiments have shown that taking into account the properties of granular material are crucial to predict the amplitude of the generated waves. The physical mechanisms involved in the collapse of an initially dry granular medium in water are particularly difficult to model. For these reasons, the numerical modeling of a granular collapse from air into water remains challenging. The modeling of a submarine collapse by solving the dynamics of each grain together with the fluid dynamics is very recent (Topin et al. 2012), and the next digital step is to add an air/water interface to the granular collapse. Therefore, the modeling of the impact of a dry granular material in water and the generated wave train still requires enormous efforts. Here, we use the software Gerris (Popinet 2003, 2009) to run numerical simulations of a situation similar to the experiments. The granular material is modeled as a fluid with non-Newtonian properties. The aim of these simulations is to reproduce the evolution of the first wave using the Navier–Stokes equations for triphasic simulations.

3.1 Parameters of the Simulations

The numerical domain is divided into three subdomains corresponding to 1 m × 1 m squares connected to each other. The slope is modeled by a solid wedge with a no-slip boundary condition. The water depth is equal to 15 cm for all the simulations. The density and viscosity of the air and water are taken for a temperature of 20 °C and a pressure 1013 hPa. To simulate different rheologies for the granular media, we have performed numerical simulations for two fluids: a Newtonian fluid ($\rho = 1500\,\mathrm{kg\,m^3}$, $\mu = 5\,\mathrm{kg.m^{-1} \cdot s^{-1}}$) and a Bingham fluid ($\rho = 1500\,\mathrm{kg.m^3}$, $\mu = 5\,\mathrm{kg.m^{-1} \cdot s^{-1}}$ and $\tau_0 = 100\,\mathrm{kg.m^{-1} \cdot s^{-2}}$).

The mesh refinement occurs at the interface between water and other fluids (air and granular material) and a constant mesh is maintained in the water and granular phases. The smallest mesh size is about 1.9 mm for the simulations presented in this article. The boundary conditions are a no-slip at the bottom, a symmetry condition at the left and right ends of the domain, and an open boundary on the top of the domain. All simulations are performed on a single processor with a computing time ranging from 6 to 12 h.

To characterize the evolution of the waves during their propagation, we set four probes at the same distances as in the experiments (0.45, 0.75, 1.05, and 1.35 m) from the point where the granular material enters the water.

3.2 Comparison of Numerical and Experimental Results

We consider the particular situation of 2 kg of glass beads of 1.5 mm in diameter sliding on a slope of 45° to quantitatively compare experiments and numerical simulations. Figure 7 shows the experimental results and the numerical simulations for two different rheologies of the slide.

We observe that the numerical simulations are in good agreement with the experiments at early times. The amplitude of the first wave during the impact is slightly larger when using a slide made of a fluid rather than a Bingham fluid. When the first wave leaves the generation region and starts to propagate, the apparition of a vortex at the edge of the slide is visible in the simulation using a Newtonian fluid. We can also observe the counter flow which slows down the collapse (see Fig. 7e). These observations are less visible in the simulation using a Bingham fluid, where the flow is slower and seems to become solid after the impact. Finally, the second wave starts to appear in a similar manner than observed in the experiments (Fig. 7g, h, i), although the slides have moved significantly less.

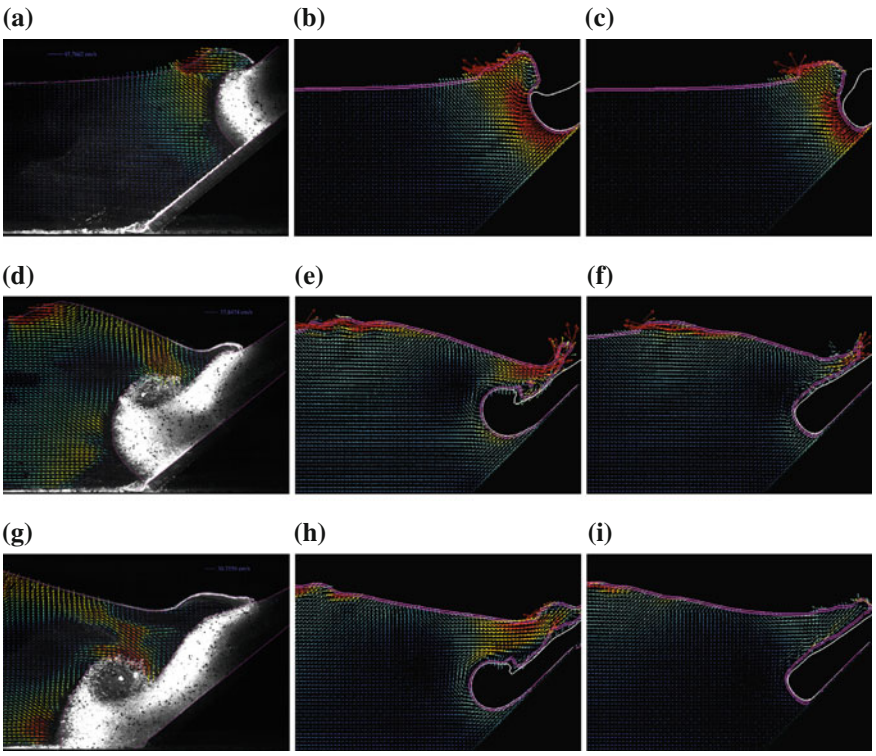

Fig. 7 Comparison between the experiments (**a**, **d**, **g**) and the numerical results obtained with Gerris using a newtonian fluid (**b**, **e**, **h**) and a Bingham rheology (**c**, **f**, **i**)

As mentioned above, numerical simulations of the granular material interacting with the fluid are really complex. For instance, the collapse of a fluid starting from air into water generates a huge vorticity and bubbles which are particularly difficult to simulate and very expensive in CPU time. Therefore, the main purpose of the present simulations is to reproduce the evolution of the amplitude of the first wave. We accordingly set the parameters of the different fluids used to simulate the slide. Apart from the density, which corresponds to the equivalent density in the experiments ($\rho_{eq} = 0.6\,\rho_g \simeq 1500\,\mathrm{kg.m^{-3}}$), the viscosity and the yield stress of the slide are not based on physical properties but rather fitted to the experiments.

3.3 Evolution of the Amplitude During Propagation

We compare the evolution of the wave amplitude between our experiments and our numerical simulations using the probes. We first need to define a rheology for the granular material and study its influence on the generated wave. We compared the wave amplitudes obtained in the experiments and in the numerical simulations for a mass $m = 2$ kg for the four types of granular materials on a slope of 45°. The simulation with a Newtonian rheology produces results in fair agreement with the experiments performed with the 4 mm glass beads, while the approximation of a Bingham fluid gives results consistent with the 1.5 mm glass beads experiments. Three configurations were considered by varying only the angle of the slope (35°, 45° and 60°). Figure 8 shows the results at the different probes for these configurations.

The evolution of the amplitude of the first wave for a slope of 45° is well captured by the numerical simulations for both the Newtonian fluid/4 mm glass beads and the Bingham fluid/1.5 mm glass beads. These first results are not surprising, since, as stated previously, the parameters of the fluids used in the numerical simulations were chosen to best match this configuration. If we now consider the results obtained for a slope of 60° we see that, once again, the numerical simulations are in relatively good agreement with the experiments. More specifically, for the Bingham fluid and the 1.5 mm glass beads, the evolution of the free surface obtained experimentally (1.5 mm glass beads) and numerically (Bingham fluid) are in close agreement for the four probes. We observe a small time offset for the second peak at the first probe which decreases during the propagation.

The largest discrepancy is observed between the amplitude of the first trough and the second crest when comparing the Newtonian fluid and the 4 mm glass beads. It shows that approximating the slide by a Newtonian fluid does not successfully reproduce the interactions between the granular material and the generated waves. However, during the propagation, the energy of the first wave is transferred to the dispersive wave train and thus the difference in amplitude at the second peak decreases. For a slope angle of 35°, the numerical simulations overestimate the amplitude of

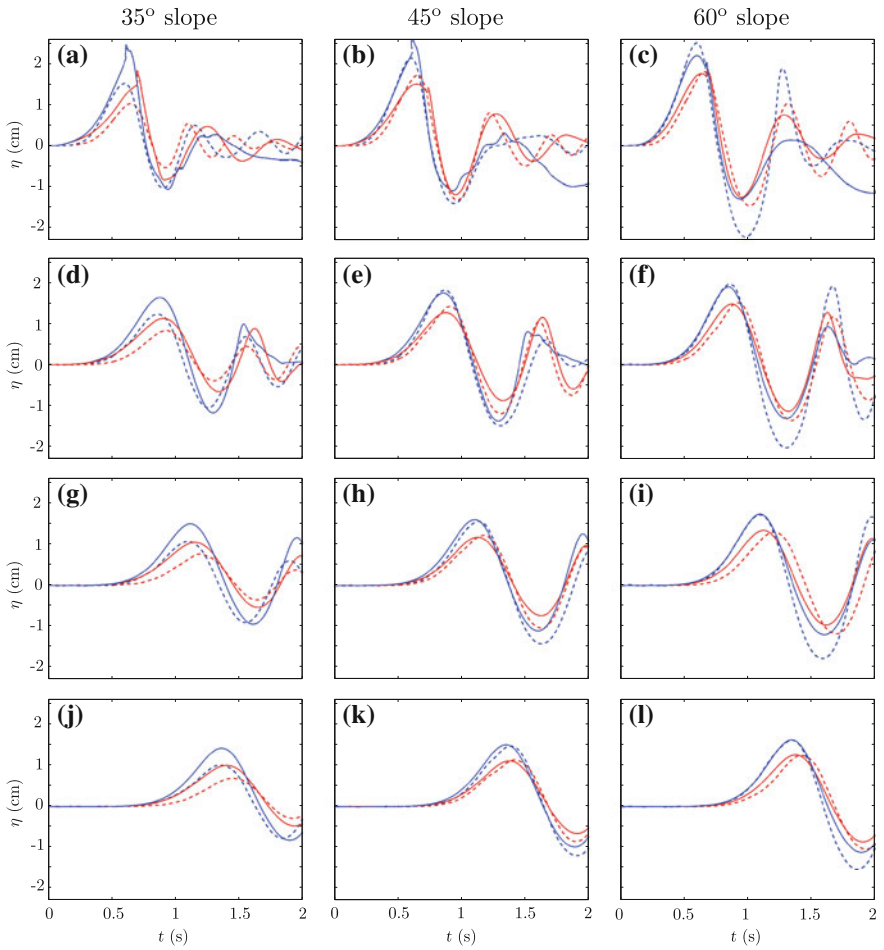

Fig. 8 Comparison of the evolution of the free surface elevation between the experiments and the numerical simulations for a slope of 35°, 45°, and 60° measured at (**a**, **b**, **c**) 0.45 m, (**d**, **e**, **f**) 0.75 m, (**g**, **h**, **i**) 1.05 m and (**j**, **k**, **l**) 1.35 m from the lifting gate. The *blue* and *red dashed lines* are experiments with 4 and 1.5 mm glass beads, respectively. The *blue* and *red* continuous line are the numerical results obtained with Gerris simulating the collapse of a Newtonian and Bingham fluid into water, respectively

the first wave and the largest discrepancies are observed in this configuration. These results are in agreement with the fact that the velocity of the slide is the lowest in this configuration. Therefore, the interactions between the granular materials and the generated waves are the most important.

4 Conclusion

From our systematic experimental study, we were able to highlight the importance of the internal properties of the granular material during its collapse into water at small Froude number. We also emphasized the importance of the interplay between the granular media and the fluid during the generation of the waves. In particular, in the configuration studied experimentally, the friction on the slope becomes dominant. Therefore, the amplitude of the generated waves does not only depend on the slope angle but on the difference between the slope angle and the avalanching angle of the granular material used. This angular dependence has also been observed for the runout distance of the granular media, which is always smaller for a granular collapse from air into water rather than for a collapse in a single fluid (air or water). We also reported that the energy transferred by the slide to the generated waves does not exceed 10 % for all initial configurations. Using numerical simulations, we then show that the approximation of a viscous fluid for the granular medium gives satisfactory results for the prediction of the amplitude of the first wave in some particular configurations, but does not satisfactory reproduce the wave train generated and the evolution of the slide. For this reason, an important experimental and numerical effort is required to understand the physical mechanisms that take place during a subaerial collapse. For instance, a numerical study using the coupling of a discrete method to simulate the granular flow (DEM) and a continuous method for the air/water phases (CFD) would lead to important informations on the energy transfer to the waves during a granular collapse into water.

Acknowledgments The authors thank Olivier Pouliquen, Pascale Aussillous, and Pierre-Yves Lagrée for many enlightening discussions. We thank Emilie Dressaire and Parmesh Gajjar for the careful reading of the manuscript and helpful comments

References

Abadie S, Morichon D, Grilli S, Glockner S (2010) Numerical simulation of waves generated by landslides using a multiple-fluid Navier-Stokes model. Coast Eng 57(9):779–794

Abadie SM, Harris JC, Grilli ST, Fabre R (2012) Numerical modeling of tsunami waves generated by the flank collapse of the cumbre vieja volcano (la palma, canary islands): tsunami source and near field effects. J Geophys Res Ocean 117(C5)

Assier-Rzadkiewicz S, Mariotti C, Heinrich P (1997) Numerical simulation of submarine landslides and their hydraulic effects. J Waterway Port Coast Ocean Eng 123(4):149–157

Averbukh E, Dussouillez P, Kharif C, Khvostova O, Kurkin A, Rochette P, Soomere T (2013) Exposure of a coastal city to a landslide tsunami: a case study of Cassis. France. Estonian J Eng 19(2):124–142

Börzsönyi T, Halsey TC, Ecke RE (2008) Avalanche dynamics on a rough inclined plane. Phys Rev E 78(1):011306

Cassar C, Nicolas M, Pouliquen O (2005) Submarine granular flows down inclined plane. Phys Fluids 17(10):103301

Choi BH, Pelinovsky E, Kim KO, Lee JS (2003) Simulation of the trans-oceanic tsunami propagation due to the 1883 Krakatau volcanic eruption. Nat Hazards Earth Syst Sci 3(5):321–332
Di Risio M, Bellotti G, Panizzo A, De Girolamo P (2009) Three-dimensional experiments on landslide generated waves at a sloping coast. Coast Eng 56:659–671
Didenkulova I, Nikolkina I, Pelinovsky E, Zahibo N (2010) Tsunami waves generated by submarine landslides of variable volume: analytical solution for a bassin of variable depth. Nat Hazards Earth Syst Sci 10(11):2407–2419
Enet F, Grilli S (2005) Tsunami landslide generation: modelling and experiments. In: Proceedings of 5th international on ocean wave measurement and analysis
Enet F, Grilli S (2007) Experimental study of tsunami generation by three-dimensional rigid underwater landslides. J Waterway Port Coast Ocean Eng 133:442–454
Enet F, Grilli ST, Watts P (2003) Laboratory experiments for tsunamis generated by underwater landslides: comparison with numerical modeling. In: Proceedings of the 13th offshore and polar engineering conference
Francis PW (1985) The origin of the 1883 Krakatau tsunami. J Volcanol Geotherm Res 25(3):349–363
Fritz HM (2002) Initial phase of landslide generated impulse waves. Ph.D. thesis, Swiss Federal Institute of Technology Zürich
Fritz HM (2001) Lituya Bay case: rockslide impact and wave run-up. Sci Tsunami Hazards 19(1):3–22
Fritz HM, Hager WH, Minor HE (2003a) Landslide generated impulse waves; part 1: instantaneous flow fields. Exp Fluids 35(6):505–519
Fritz HM, Hager WH, Minor HE (2003b) Landslide generated impulse waves; part 2: hydrodynamic impact craters. Exp Fluids 35(6):520–532
Fritz HM, Hager WH, Minor HE (2004) Near field characteristics of landslide generated impulse waves. J Waterway Port Coast Ocean Eng 130(6):287–302
Fritz HM, Mohammed F, Yoo J (2009) Lituya Bay landslide impact generated mega-tsunami 50th anniversary. Pure Appl Geophys 166(1–2):153–175
Gisler GR, Weaver RP, Mader CL, Gittings ML (2004) Two and Three dimensional simulation of asteroid ocean impacts. Sci Tsunami Hazards 21(2):119
Glimsdal S, Pedersen GK, Harbitz CB, Lovholt F (2013) Dispersion of tsunamis: does it really matter? Nat Hazards Earth Syst Sci 13:1507–1526
Grilli ST, Vogelmann S, Watts P (2002) Development of a 3D numerical wave tank for modeling tsunami generation by underwater landslides. Eng Anal Bound Elem 26(4):301–313
Grilli ST, Watts P (1999) Modeling of waves generated by a moving submerged body. Applications to underwater landslides. Eng Anal Boundy Elem 23(8):645–656
Grilli ST, Watts P (2005) Tsunami generation by submarine mass failure part I: modeling, experimental validation, and sensitive analysis. J Waterway Port Coast Ocean Eng 131(6):283–297
Heinrich P (1992) Nonlinear water waves generated by submarine and aerial landslides. J Waterway Port Coast Ocean Eng 118(3):249–266
Heller V, Hager WH (2014) A universal parameter to predict subaerial landslide tsunamis? J Mar Sci Eng 2:400–412
Heller V, Hager WH, Minor HE (2008) Scale effects in subaerial landslide generated impulse waves. Exp Fluids 44(5):691–703
Ioualalen M, Asavanant J, Kaewbanjak N, Grilli ST, Kirby JT, Watts P (2007) Modeling the 26 December 2004 Indian ocean tsunami: case study of impact in Thailand. J Geophys Res Oceans 112(C7)
Kelfoun K, Giachetti T, Labazuy P (2010) Landslide-generated tsunamis at Réunion Island. J Geophys Res Earth Surf 115:F4
Kharif C, Pelinovsky E (2005) Asteroid impact tsunami. Comptes Rendus Physique 6(3):361–366
Korteweg DJ, De Vries G (1895) On the change of form of long waves advancing in a rectangular canal, and on new type of long stationary waves. Phil Mag 39(240):422–443

Liu PF, Wu TR, Raichlen F, Synolakis CE, Borrero JC (2005) Runup and rundown generated by three-dimensional sliding masses. J Fluid Mech 536:107–144
Mader CL, Gitting ML (2002) Modeling the 1958 Lituya Bay mega-tsunami. II. Sci Tsunami Hazards 20(5):241–250
Mohammed F (2010) Physical modeling of tsunamis generated by three-dimensional deformable granular landslides. Ph.D. thesis, Georgia Institute of Technology, December 2010
Mohammed F, Fritz HM (2012) Physical modeling of tsunamis generated by three-dimensional deformable granular landslides. J Geophys Res Oceans 117:C11015
Monaghan JJ, Kos A (2000) Scott Russell's wave generator. Phys Fluids 12(3):622–630
Murty TS (1979) Submarine slide generated water waves in Kitimat Inlet, British Columbia. J Geophys Res Oceans 84(C12):7777–7779
Panizzo A, De Girolamo P, Petaccia A (2005) Forecasting impulse waves generated by subaerial landslides. J Geophys Res Oceans 110:C12025
Pelinovsky E, Talipova T, Kharif C (2000) Nonlinear-dispersive mechanism of the freak wave formation in shallow water. Phys D : Nonlinear Phenom 147(1–2):83–94
Popinet S (2003) Gerris: a tree-based adaptive solver for the incompressible Euler equations in complex geometries. J Comput Phys 190(2):572–600
Popinet S (2009) An accurate adaptive solver for surface-tension-driven interfacial flows. J Comput Phys 228(16):5838–5866
Popinet S (2011) Quadtree-adaptive tsunami modelling. Ocean Dyn 61(9):1261–1285
Pouliquen O (1999) Scaling laws in granular flows down rough inclined planes. Phys Fluids 11(3):542–548
Quecedo M, Pastor M, Herreros MI (2004) Numerical modeling of impulse wave generated by fast landslides. Int J Numer Methods Eng 59(12):1633–1656
Sælevik G, Jensen A, Pedersen G (2009) Experimental investigation of impact generated tsunami; related to a potential rock slide. Western Norway. Coast Eng 56(9):897–906
Scott Russel J (1844) Report on Waves. In: Report of the 14th meeting of the British Assocaition for the Advancement of Science, vol 311, pp. 390
Shi F, Kirby JT, Harris JC, Geiman JD, Grilli ST (2012) A High-order adaptive time-stepping TVD solver for Boussinesq modeling of breaking waves and coastal inundation. Ocean Model 43:36–51
Shi F, Kirby JT, Tehranirad B, Harris JC, Grilli ST (2011) FUNWAVE-TVD, Fully nonlinear Boussinesq wave model with TVD solver, documentation and user's manual (Version 2.1). Technical report, Center for Applied Coastal Research, University of Delaware
Tinti S, Bortolucci E (2000) Energy of water waves induced by submarine landslides. Pure Appl Geophys 157(3):281–318
Topin V, Monerie Y, Perales F, Radjai F (2012) Collapse dynamics and runout of dense granular materials in a fluid. Phys Rev Lett 109(18):188001
Viroulet S, Cébron D, Kimmoun O, Kharif C (2013) Shallow water waves generated by subaerial solid landslides. Geophys J Int 193(2):747–762
Viroulet S, Sauret A, Kimmoun O (2014) Tsunami generated by a granular collapse down a rough inclined plane. Europhys Lett 105(3):34004
Viroulet S, Sauret A, Kimmoun O, Kharif C (2013a) Effondrement granulaire dans l'eau: application à la génération de tsunami. In: 21eme Congrès Francais de Méecanique, Bordeaux, France
Viroulet S, Sauret A, Kimmoun O, Kharif C (2013b) Granular collapse into water: toward tsunami landslides. J Visualization 16(3):189–191
Walder JS, Watts P, Sorensen OE, Janssen K (2003) Tsunamis generated by subaerial mass flows. J Geophys Res Solid Earth 108(B5)
Wang Y, Liu PLF, Mei CC (2011) Solid landslide generated waves. J Fluid Mech 675:529–539
Watts P (1997) Water waves generated by underwater landslides. Ph.D. thesis, California Institute of Technology
Watts P (1998) Wavemaker curves for tsunamis generated by underwater landslides. J Waterway Port Coast Ocean Eng 124(3):127–137

Watts P (2000) Tsunami features of solid block underwater landslides. J Waterway Port Coast Ocean Eng 126(3):144–152
Watts P, Grilli ST, Kirby JT, Fryer GJ, Tappin DR (2003) Landslide tsunami case studies using a Boussinesq model and a fully nonlinear tsunami generation model. Nat Hazards Earth Syst Sci 3(5):391–402
Whitham GB (2011) Linear and nonlinear waves, vol 42. John Wiley & Sons
Zweifel A, Hager WH, Minor HE (2006) Plane impulse waves in reservoirs. J Waterway Port Coast Ocean Eng 132(5):358–368